Journal of Power Sources 196 (2011) 8669–8674

Contents lists available at ScienceDirect

Journal of Power Sources

journal homepage: www.elsevier.com/locate/jpowsour

Facile synthesis and electrochemical properties of Fe_3O_4 nanoparticles for Li ion battery anode

Shantanu K. Behera*

Department of Mechanical Engineering, University of Colorado at Boulder, Boulder, CO 80303, USA

ARTICLE INFO

Article history:
Received 6 May 2011
Received in revised form 15 June 2011
Accepted 16 June 2011
Available online 28 June 2011

Keywords:
Magnetite
Li ion battery
Anode
Nanoparticles
Iron oxide

ABSTRACT

Nanostructured Fe_3O_4 nanoparticles were prepared by a simple sonication assisted co-precipitation method. Transmission electron microscopy, X-ray diffraction and BET surface area analysis confirmed the formation of ~20 nm crystallites that constitute ~200 nm nanoclusters. Galvanostatic charge–discharge cycling of the Fe_3O_4 nanoaprticles in half cell configuration with Li at 100 mA g^{-1} current density exhibited specific reversible capacity of 1000 mAh g^{-1}. The cells showed stability at high current charge–discharge rates of 4000 mA g^{-1} and very good capacity retention up to 200 cycles. After multiple high current cycling regimes, the cell always recovered to full reversible capacity of ~1000 mAh g^{-1} at 0.1 C rate.

1. Introduction

Li ion batteries (LIB) are, by far, the most promising of all secondary storage devices. Growing demand for high energy density and high power density batteries has shifted the attention from graphitic anodes, with a theoretical capacity of 372 mAh g^{-1}, to many oxides, alloys and hybrid materials with higher specific capacity. Recently, it has been shown that transition metal oxides possessing reversible capacity between 600 and 1000 mAh g^{-1} can potentially replace graphite based anodes [1]. In particular, Fe_3O_4 exhibits promise since it possesses high specific capacity, is cheap, abundantly available, and environmentally benign [2,3]. Magnetite also possesses good electronic conductivity of 2×104 S m^{-1}, which is considerably better than other transition metal oxides [4]. Although the results are promising, capacity retention after several cycles and the ability to operate at higher current densities are some of the concerns that need to be bettered. In general, anode materials with higher specific capacity tend to undergo considerable amount of volume dilation between the Li^+ inserted and extracted states. For Fe_3O_4 based anodes the active materials transform from an oxide to metallic iron. Such volume changes result in pulverization of the active materials, disintegration of the anode assembly, poor cycling performance, and capacity fade over several charge discharge cycles [5]. Battery anodes with nanostructured materials have significant advantages [6] because of (i) short Li ion transport distance, (ii) large electrolyte-electrode contact area that provides faster reactions, and (iii) accommodation of the structural strain generated due to Li intercalation. Therefore, to improve the electrochemical properties of LIB anodes, Fe-oxide based nanostructured materials [7–12], composites and hybrids [13–22] have been considered. Taberna et al. deposited Fe_3O_4 on Cu nanorods and obtained 800 mAh g^{-1} capacity cycling at C/32 rate [3]. Recently, Wang et al. produced sub-micron spheroids of magnetite that delivered 900 mAh g^{-1} capacity for up to 60 cycles [10]. On the contrary, however, Chen et al. showed that microcrystalline Fe_3O_4 exhibited better capacity retention (685 mAh g 1 at 50th cycle) than nanocrystalline Fe_3O_4 [11]. With Fe_3O_4 and carbon based composites Zhang et al. and Liu et al. obtained capacity in the range of 600 mAh g^{-1} that were stable over 50 cycles [8,14]. Some of the very recent literatures have shown graphene–magnetite composites with good cyclic stability and rate capability [16–22].

Design of an efficient anode configuration can be accomplished in two stages. Crystallinity, morphology, size and the distribution of the active oxide materials have a profound influence on the performance of the battery; it has been shown specifically in the iron oxide system [23,24]. Therefore, optimization of the nanoparticle parameters can lead to better capacity, rate capability and cyclic stability. Secondly, with the use of new admixtures, including graphene, carbon nanotubes (CNT), core-shell assemblies, etc., the cell performance can be bettered further [15,20–22]. The current work underscores the first approach, and describes an easy and inexpensive process for the synthesis of Fe_3O_4 nanoparticles. Synthesis of oxide materials by co-precipitation process is a very

* Corresponding author at: National Institute of Technology Rourkela, INDIA 769008 Tel.: +91 8658588058.
E-mail address: SKB204@alumni.lehigh.edu

0378-7753/$ – see front matter © 2011 Elsevier B.V. All rights reserved.
doi:10.1016/j.jpowsour.2011.06.067

well established and inexpensive technique that has the potential for processing of bulk amounts of nanostructured materials [25]. In the current work, a novel ultrasonic assisted co-precipitation method has been used to synthesize magnetite nanoparticles with controlled size, morphology and distribution. The said magnetite nanoparticles were found to deliver excellent specific reversible capacity of 1000 mAh g^{-1} at 0.1 C, sustain cycling at extremely high current density (4000 mA g^{-1}), and exhibit stability up to at least 200 cycles without capacity fading.

2. Experimental

2.1. Nanoparticle synthesis

An inexpensive, sonication assisted co-precipitation method that has been tried in other systems [26] was applied for the synthesis of Fe_3O_4 nanoparticles. Fe^{3+} and Fe^{2+} chlorides (Alfa Aesar) were mixed at the molar ratio of 2:1 in deionized water. The solution was destabilized with the addition of 1 M NaOH solution while maintaining the pH of the system between 8 and 10. The contents in the beaker were irradiated with an ultrasonic horn (20 kHz) for 30 min to yield a blackish suspension. The nanoparticles were separated from the suspension by a research centrifuge operated at 4000 rpm, re-dispersed in distilled water inside an ultrasonic bath and recollected by the centrifuge. The process of ultrasonic washing and centrifugal washing was carried out for 5–6 times before the final filtrate was collected.

2.2. Powder characterization

Transmission electron microscopy (TEM, 2000FX JEOL, Japan) was performed to study the size and morphology of the nanoparticles. A drop of the colloid was placed on a polymer coated Cu grid (Ted Pella), dried under heat lamp and was observed in bright field (BF) mode at an accelerating voltage of 200 kV. Selected area diffraction (SAD) pattern was collected on a cluster of the nanoparticles in TEM. Crystallography of the nanoparticles was determined by an X-ray diffractometer (Philips PW1730, Philips, Eindoven, Netherlands) with Cu-K_α radiation (λ = 1.54056 Å) operated at a scan rate of 2° min^{-1} between 20° and 80° of 2Θ. X-ray line broadening technique was used to calculate the crystallite size of the magnetite powders with Si as internal standard using Scherrer's formula:

$$D = \frac{0.889\lambda}{\beta \cos \Theta_B} \quad (1)$$

where D is the crystallite size, λ is the X-ray wavelength, β is the full width at half maximum (FWHM), and Θ_B is the diffraction half angle corresponding to the maximum intensity peak. In this case, the maximum intensity corresponds to (3 1 1) family of planes. N_2 adsorption–desorption isotherms of the magnetite nanoparticles were collected at 77 K with relative pressure P/P_0 between 0.05 and 0.99 (Micromeritics ASAP 2010, Norcross, GA, USA). Samples were degassed at 220 °C overnight before analysis. Specific surface area was computed by the Brunauer–Emmet–Teller (BET) model. Barrett–Joyner–Halenda (BJH) model was applied to calculate the pore size distribution and pore volume.

2.3. Electrochemical characterization

The electrochemical response was measured with CR-2032 type coin cell assembly in half cell configuration. First the Fe_3O_4 nanoparticles, acetylene black, and poly-vinylidenedifluoride (PVdF) were mixed in a ratio of 60:20:20 with the help of N-methyl-2-pyrrolidinone in an acid washed agate mortar. The slurry was cast onto a Cu foil (Goodfellow) by doctor-blade process, dried in an oven, and circular electrodes were punched out. Then the electrodes were baked in a furnace (Thermolyne, IA) at 450 °C for 1 h in flowing Ar. Li foil (Alfa Aesar) was used as the counter electrode for the cell. $LiPF_6$ (1 M) dissolved in a solution of ethylene carbonate (EC) and dimethyl carbonate (DMC) in 1:1 ratio (Novolyte, USA) was used as the battery electrolyte. Trilayered polymeric microporous membranes (Celgard, USA) soaked in the electrolyte was used as the separator between the working electrode and Li foil. The half cells were layer-assembled, punched and crimped inside a glove box with <1 ppm of moisture and oxygen levels. Galvanostatic charge–discharge cycles were recorded between the 0.01 V and 3 V window in a battery tester (BT-2000, Arbin Instruments) with current densities varying between 100 and 4000 mA g^{-1}, following symmetric cycling. Half cells were made with commercial microcrystalline magnetite particles and tested to compare the electrochemical behavior of the magnetite nanoparticles.

3. Results

3.1. Nanoparticles synthesis

The washed nanoparticles were such that they can be peptized with water without the use of any surfactant to make a nanocolloid that remains stable for months. The dried Fe_3O_4 nanoparticles, however, were powders with a monomodal size distribution, as can be seen from the TEM micrographs (cf. Fig. 1a). The SAD pattern shows well defined concentric rings, indicating that the powders are crystalline and not amorphous (inset of Fig. 1a). Absence of spots in the SAD pattern also indicated that the crystallite size is fine. At a higher magnification (cf. Fig. 1b), however, it can be seen that the individual crystallites are of <20 nm size. Because of the high surface energy associated with the small diameter the dried nanopowders remain as clusters of ~200 nm size (Fig. 1a). The powder morphology can be best described as multiple nanocrystallites clustering together to form slightly bigger nanoparticles. X-ray diffractogram of the nanoparticles (cf. Fig. 2) calcined at 450 °C indicated characteristic peaks of the FCC lattice. The peak positions and intensity could be correlated to Fe_3O_4 inverse spinel structure based on JCPDS file card no. 85-1436. The crystallite size of the powders, as calculated by Scherrer's formula, was 24 nm, which is in close agreement with the TEM micrographs. The N_2 sorption isotherms (Fig. 3) exhibited very small, but visible, area of hysteresis between the adsorption and desorption branches. This feature indicates that the nanoparticles have some amount of mesoporosity (pore size between 2 nm and 50 nm). The BET specific surface area of the nanopowders was 27 g m^{-2}. BJH pore model calculations indicated an average pore size of 24 nm. All in all, the TEM micrographs, crystallite size calculations from X-ray line broadening and the average pore size value are in agreement.

3.2. Electrochemical capacity

To test the electrochemical behavior of the anodes at moderate current rates, the first few insertion–extraction cycles were carried out at 100 mA g^{-1} current density. The voltage profile for the first insertion cycle had three distinct features (cf. Fig. 4) The step voltage drop from 3 to 0.75 V refers to the formation of a Li–Fe–O complex (cf. Eq. (2)). The subsequent voltage plateau at ~0.75 V refers to the conversion reaction of the Li–Fe–O complex to Fe and Li_2O (cf. Eq. (3)). The gradual voltage decay from 0.7 V to 0.01 V corresponds to the formation of a gel like anode electrolyte interface [27].

$$Fe_3O_4 + xLi = Li_xFe_3O_4 \quad (2)$$

$$Li_xFe_3O_4 + (8 - x)Li = 3Fe + 4Li_2O \quad (3)$$

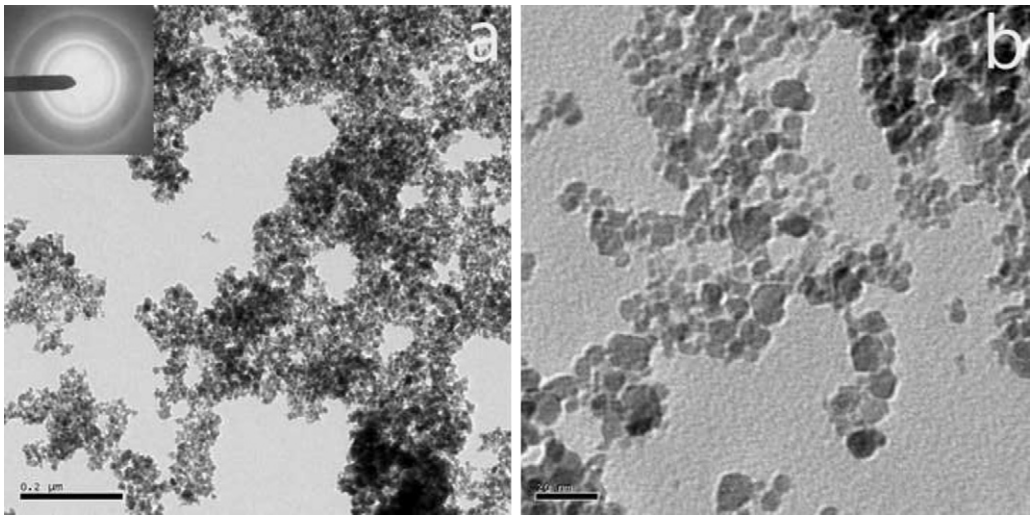

Fig. 1. Transmission electron micrograph of the Fe_3O_4 nanoparticles; (a) low magnification image indicating nanoclusters of magnetite (scale bar is 200 nm), inset image is the SAD pattern-absence of spots and well-defined ring patterns indicate formation of nanocrystallites; (b) high magnification image showing individual crystallites of 10 nm or less in dimension (scale bar is 20 nm).

The first cycle delivered a total capacity of 1470 mAh g^{-1} during the insertion half, while the reversible capacity was 1085 mAh g^{-1}. The capacity obtained is significantly better than the values reported in recent literature for magnetite or magnetite-based composites [7–12]. If we considered the contribution of carbon black, which was used as a conductive agent, the specific reversible capacity for Fe_3O_4 would still be ~1000 mAh g^{-1}. The irreversible capacity loss (ICL) was 26%, which is in agreement or better than previous reports in magnetite based anodes. After the first cycle, however, the voltage profiles during cycling showed only two prominent portions, which remain unchanged (up to at least 200 cycles in the current study).

3.3. Rate capability

Rate capability is an important aspect of the development of current generation battery electrodes. To test the rate capability the cell was cycled at progressively increasing current densities following symmetric rates of charge and discharge.[1] The rates were increased starting with 100 mA g^{-1}, to 200, 400, 800, 1600, 2000, and as high as 4000 mA g^{-1} (cf. Fig. 5); the resulting reversible capacities delivered by the cell were 1085 mAh g^{-1}, 980 mAh g^{-1}, 858 mAh g^{-1}, 560 mAh g^{-1}, 300 mAh g^{-1}, 240 mAh g^{-1}, and 200 mAh g^{-1}, respectively. These current densities span from moderate (0.1 C) to high C-rates (5 C). The reversible capacities obtained in this study, for both moderate and high C-rates, are considerably better than that of graphitic anodes. In all of the cycles the coulombic efficiency was close to 100%. The most important result was the recovery of the cell after extreme rate cycling. When the current density was brought back to 100 mA g^{-1} after 5 charge–discharge cycles at 4000 mA g^{-1}, the cell recovered full capacity of 1084 mAh g^{-1} at 0.1 C rate. This indicates the stability of the anode in a wide range of current rate.

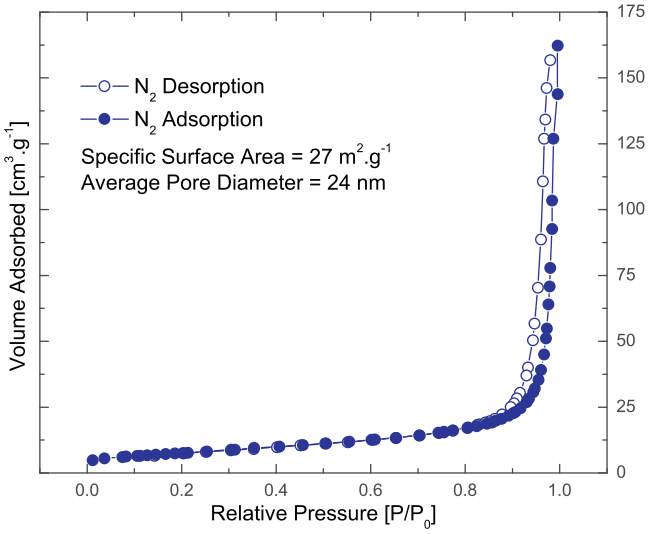

Fig. 3. N_2 adsorption–desorption isotherms at 77 K. Existence of mesopores (between 2 and 50 nm) is indicated by the small hysteresis between the two branches in the isotherm.

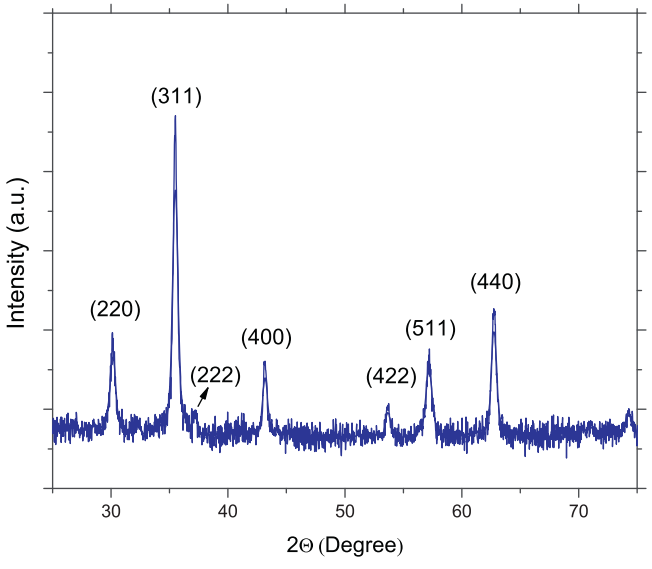

Fig. 2. X-ray diffraction pattern of the magnetite nanoparticles. Diffracting planes are indicated in parentheses.

[1] During symmetric cycling the current applied is kept the same during the Li insertion and extraction halves. It delivers lower specific capacity than in asymmetric current cycling, where Li insertion is carried out slowly (~0.1 C) followed by extraction at desired fasterrates.

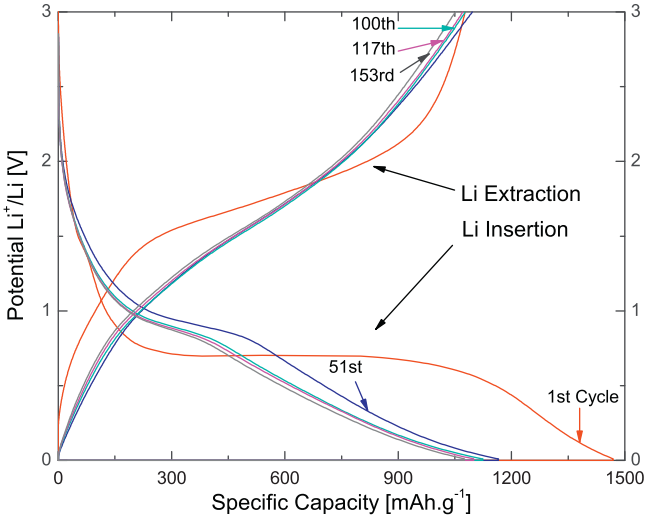

Fig. 4. Galvanostatic charge–discharge cycles of the cell at 100 mA g^{-1} current density between 0.01 V and 3 V. The cycle numbers are indicated in the figure.

Another cell of the same anode composition was cycled at an aggressive current rate of 2000 mA g^{-1}, equivalent to 2 C rate. As can be seen in Fig. 6, the cell delivered ~900 mAh g^{-1} capacity. The capacity retention at the end of 20 cycles was extremely good. On the contrary, the cell made with microcrystalline magnetite anode (average particle size of 5 μ) showed rapid decay in capacity. At the end of the 10th cycle, the specific capacity had already reduced to 10% of the original reversible capacity. It may be noted that the microcrystalline magnetite the cycling was carried out at a moderate current density of 200 mA g^{-1}, which roughly corresponds to 0.2 C rate. On a comparison, the nanostructured magnetite anodes showed very good cyclic stability, although the cycling rate was an order of magnitude higher than that of the microcrystalline anodes. These results indicate the exceptional stability of the anode to high rates of Li insertion and extraction.

3.4. Cyclic stability

To study the cyclic stability of the anodes, the cell was tested for additional 100 cycles at higher charge–discharge rates, e.g. at 1 C, 5 C and 1.5 C (cf. Fig. 7). The cell cycled at 1 C rate for 50 cycles (cf. Fig. 7) show virtually no fading of capacity. The coulombic efficiency

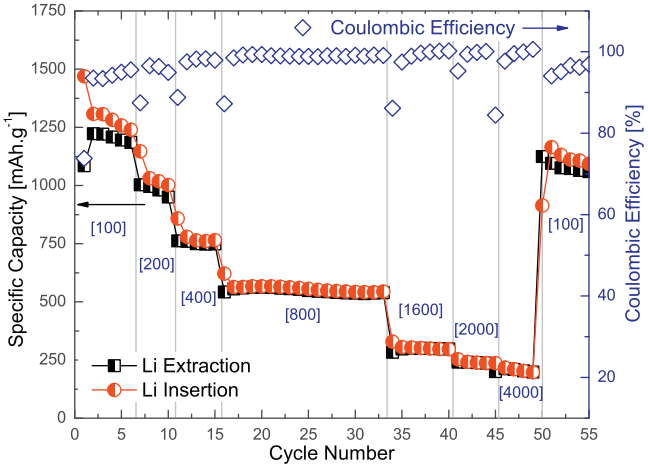

Fig. 5. Specific charge and discharge capacity of the cell and coulombic efficiency for the first 55 cycles with step-wise increase in current. Numbers in the square brackets show current density for the cycles in mA g^{-1}.

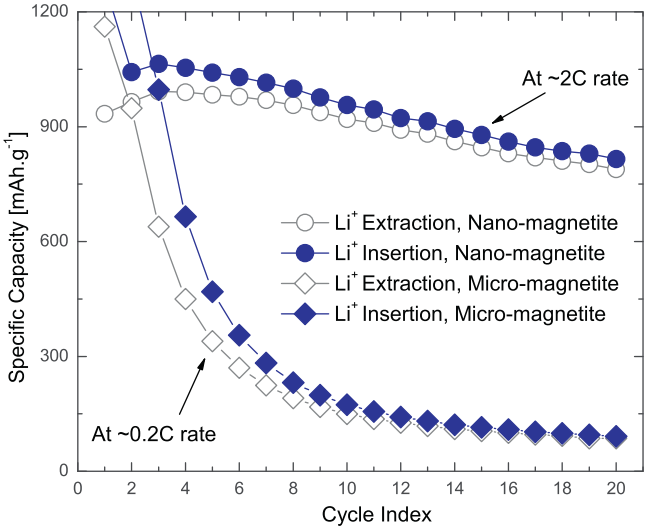

Fig. 6. Comparison of Li^+ intercalation ability of nanosized and microsized magnetite nanoparticles. Note that the nanoparticulate Fe_3O_4 has been cycled at 2000 mA g^{-1} current density, whereas the micron sized Fe_3O_4 particles have been cycled at a moderate current density of 200 mA g^{-1}. The capacity retention and cyclic ability of the nano-Fe_3O_4 is clearly evident despite an order of magnitude difference in the current rate.

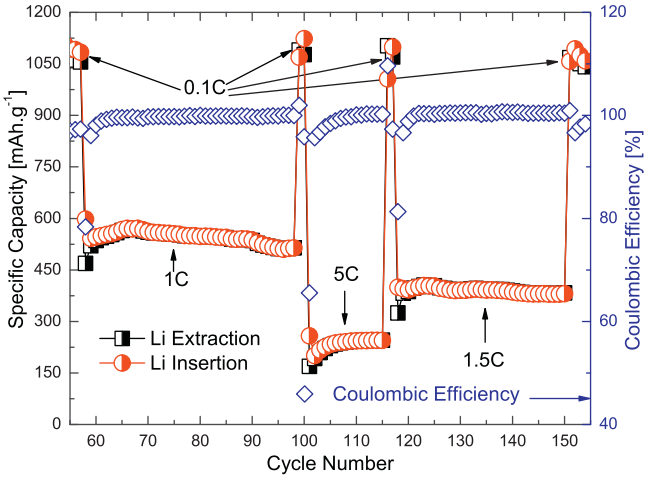

Fig. 7. Charge–discharge capacity and cyclic stability (symmetric cycling) test at higher current densities (i.e. higher C-rate) for the cells. Note that intermittent charge–discharge at low C-rate (0.1 C) recovers full capacity of the cell.

also was 100% consistently. Subsequent cycling at 100 mA g^{-1} (i.e. 0.1 C) produced reversible capacity of 1084 mAh g^{-1} (cycle no. 100 in Fig. 7), similar to the values obtained during the initial cycling of the cells at 0.1 C. Additional cycling of the cells at 5 C and 1.5 C rates also showed consistent capacity and coulombic efficiency. More importantly, during intermittent cycling at lower rates (at 0.1 C) the cells always recovered the specific capacity of >1000 mAh g^{-1}. It may be observed that the voltage–capacity profiles of the 51st, 100th, 117th, and 153rd cycles are almost similar (cf. Fig. 4), and that there is no degradation of capacity over such long cycling (cf. Fig. 7). These results underscore the robust and structurally stable form of the nanoparticles.

4. Discussion

A few features come out strikingly different in the current set of experiments as compared to the electrochemical behavior of Fe_3O_4 based conventional anode materials in the literature. Based

on Eqs. (2) and (3), the theoretical capacity for Fe_3O_4 is 924 mAh g^{-1} considering transfer of 8 electrons per formula weight. The specific capacity obtained in the current study (1000 mAh g^{-1}) seems slightly higher than the theoretical value. Although rarely seen for intercalation mechanism based anodes (graphite), origin of such additional capacity (values above the theoretical capacity for the structure) have been observed in literature for nanostructured transition metal oxide based anodes, including magnetite–carbon core–shell anodes [14], magnetite–carbon nanotube hybrid anodes [15], and CoO based thin film electrodes [28]. Laruelle et al. have proposed that formation of a polymeric film by the decomposition of the electrolyte plays an important role in the capacity increase [27]. This pseudocapacitive layer only forms during 0.01–1.8 V region, and is not stable during cycling at higher voltages. The formation and disappearance of the polymeric layer may be thought of as an additional electroactive component of the anode structure that increases the capacity.

The current work showed considerably better cyclic stability amongst similar cells made from nanoparticles, carbon black and binders [7,10,29]. Although results by Wang et al. are comparable to the current set of electrochemical properties, the anode composition used in their study was much different [10]. Compared to the low amount of active oxides and higher amount of conducting additives and binders (40% magnetite, 30% each of binder and carbon black) used by Wang et al. the current work had a composition with 60% magnetite. Stability up to 200 cycles, recovery of full capacity after multiple times of high current cycling can be regarded as considerable improvements in the electrochemical properties of a conventional anode composition. Additionally, the results are as good as anodes made of magnetite and special additives including graphene, nanotubes and core/shell structures [14,16–22]. Graphene and/or CNT act as conducting agents and structural buffers in the anode structure thereby imparting high rate capability and structural stability. But the current results, based on a conventional anode configuration, indicate that control of nanoparticle size and morphology can significantly improve cell performance. Use of special additives with the nanoparticles of the current study can improve cell properties even more; such experiments are underway and are subjects of future communication.

The excellent cyclic stability and capacity retention of the magnetite based anode owe to the nanodimensional structure of the materials. Rate capacity directly results from the transport advantage of the Li^+ ions. For high rate capability the diffusion length of Li ions should be minimized and the diffusion coefficient should be maximized. Smaller size of the active materials directly brings down the mean diffusion time (smaller diffusion length) thereby enabling high rate intercalation. The high surface area of the nanoparticles increases the electrode–electrolyte contact area that supports faster diffusion. Additionally, the high specific surface area of the powders effectively reduces the current density (mA m^{-2}) of the active materials, which explains the ability of the Fe_3O_4 nanoparticles to sustain current density as high as 4000 mA g^{-1}. Li sequestration in Fe_3O_4 anodes is a conversion process (cf. Eqs. (2) and (3)), where Li^+ uptake essentially forms a composite of Fe and Li_2O [1]. The two states of Fe (that of an oxide and a metal) during charged and discharged states bring about large volume changes. The nanostructured morphology of the active oxides, in the current study, provided ample free volume to absorb the stress and volume dilation associated with fast cycling of Li ions.

The control of particle morphology and size distribution can be difficult during the synthesis of oxide materials by co-precipitation process since kinetic factors govern growth of particles. Generally, the process is controlled by two steps; nucleation of the precipitating phase occurs when the concentration of the species reach supersaturation, and slow growth of the nuclei by the diffusion of the solute to the crystal surface (either diffusion limited growth or interface limited growth). For the synthesis of monodispersed particles, these two steps need to be separated [30]. During the ultrasonic irradiation, the generation of very high local temperatures, caused by the rapid collapse of ultrasonic cavities, converts the salts into oxides. Sonication aids nucleation of many sites, but the growth process is disturbed. Thus a well dispersed monomodal distribution of oxide crystallites is achieved [31,32].

Magnetite is very sensitive to air. During the processing steps including centrifugal washing, filtration and drying, it may be possible that a portion of the nanopowders may have oxidized to form γ-Fe_2O_3 (maghemite). The baking of the electrodes at 450 °C in neutral atmosphere (Ar) presumably serves two purposes. First, it ensures the loss of small amount of $Fe(OH)_2$ that may be present in the powders, and the nanopowders are stabilized back in the Fe_3O_4 spinel structure. This could not be conclusively ascertained from transmission electron microscopy studies on the baked and unbaked anode fragments; both samples were virtually similar. This may be because TEM analysis is typically not very sensitive to surface hydroxides. Use of surface sensitive techniques, such as X-ray photoelectron spectroscopy may aid our understanding. However, observation by the naked eye itself lends support to the existence of small amount of oxide forms other than magnetite. The unbaked anode assembly appeared very slightly reddish as compared to the fully black appearance of the baked anodes, indicating the complete conversion to magnetite. Additionally, the baking of the anode assembly rather than free Fe-oxide nanopowders keeps the nanoparticulate size of the active oxides. Calcination of the free Fe-oxide powders may initiate coarsening, thus diminishing the size advantage. On the other hand the anode assembly, an intimate mixture of nanopowders, carbon black and binder, provides less direct diffusion paths and limits the coarsening of the active oxide.

5. Summary

A facile bulk synthesis route was followed to produce monomodal magnetite nanoparticles of ~10 nm. Electrochemical characterization of the nanopowders for Li ion battery anodes showed reversible capacity of ~1000 mAh g^{-1} for charge–discharge rates at 0.1 C. Progressive increase in the current showed that the cell can cycle at 4000 mA g^{-1} current density and deliver reversible capacity of 200 mAh g^{-1}. The cells showed no fading of capacity for at least 200 charge–discharge cycles, and always recovered full reversible capacity of ~1000 mAh g^{-1} at 0.1 C rate after high current cycling. The consistent result of specific capacity higher than the theoretical capacity of Fe_3O_4 based anode was presumably because of the catalytically enhanced reduction of the electrolyte forming a pseudocapacitive lithium active polymeric layer. The excellent cyclability, capacity retention and rate capability of the anode is due to the nanometric size and narrow distribution of the magnetite particles.

Acknowledgements

The author is indebted to Prof. Martin Harmer (Lehigh University) and Prof. Rishi Raj (University of Colorado at Boulder) for their encouragement to pursue independent work. The Fe_3O_4 nanoparticles were prepared at Lehigh University, and the electrochemical tests were carried out at the University of Colorado at Boulder.

References

[1] P. Poizot, S. Laruelle, S. Grugeon, L. Dupont, J.M. Tarascon, Nature 407 (2000) 496.
[2] S. Mitra, P. Poizot, A. Finke, J.M. Tarascon, Adv. Funct. Mater. 16 (2006) 2281–2287.
[3] P.L. Taberna, S. Mitra, P. Poizot, S. Simon, J.M. Tarascon, Nat. Mater. 5 (2006) 567.

[4] J.M.D. Coey, A.E. Berkowitz, L. Balcells, F.F. Purtis, F.T. Parker, App. Phys. Lett. 72 (1998) 734–736.
[5] Y. Idota, T. Kubota, A. Matsufuji, Y. Maekawa, T. Miyasaka, Science 276 (1997) 1395.
[6] A.S. Arico, P. Bruce, B. Scrosati, J.M. Tarascon, W.V. Schalkwijk, Nat. Mater. 4 (2005) 366–367.
[7] H. Duan, J. Gnanaraj, X. Chena, B. Li, J. Liang, J. Power Sources 185 (2008) 512–518.
[8] W.M. Zhang, X.L. Wu, J.S. Hu, Y.G. Guo, L.J. Wan, Adv. Funct. Mater. 18 (2008) 3941–3946.
[9] Z.-M. Cui, L.-Y. Jiang, W.-G. Song, Y.-G. Guo, Chem. Mater. 21 (2009) 1162–1166.
[10] S. Wang, J. Zhang, C. Chen, J. Power Sources 195 (2010) 5379–5381.
[11] Y.X. Chen, L.H. He, P.J. Shang, Q.L. Tang, Z.Q. Liu, H.B. Liu, L.P. Zhou, J. Mater. Sci. Technol. 27 (2011) 41–45.
[12] M.-S. Wu, Y.-H. Ou, Y.-P. Lin, J. Electrochem. Soc. 158 (2011) A231–A236.
[13] L. Wang, Y. Yu, P.C. Chen, D.W. Zhang, C.H. Chen, J. Power Sources 183 (2008) 717–723.
[14] H. Liu, G. Wang, J. Wang, D. Wexler, Electrochem. Commun. 10 (2008) 1879–1882.
[15] C. Ban, Z. Wu, D.T. Gillaspie, L. Chen, Y. Yan, J.L. Blackburn, A.C. Dillon, Adv. Mater. 22 (2010) E145–E149.
[16] G. Zhou, D.-W. Wang, F. Li, L. Zhang, N. Li, Z.-S. Wu, L. Wen, G. Qing, M. Lu, H.-M. Cheng, Chem. Mater. 22 (2010) 5306–5313.
[17] K. Zhou, Y. Zhu, X. Yang, C. Li, New J. Chem. 34 (2010) 2950–2955.
[18] Y. Piao, H. Sik, Y.-E. Sung, T. Hyeon, Chem. Commun. 46 (2010) 118–120.
[19] M. Zhang, D. Lei, X. Yin, L. Chen, Q. Li, Y. Wang, T. Wang, J. Mater. Chem. 20 (2010) 5538–5543.
[20] P. Wu, N. Du, H. Zhang, J. Yu, D. Yang, J. Phys. Chem. C 115 (2011) 3612–3620.
[21] B. Li, H. Cao, J. Shao, M. Qu, J.H. Warner, J. Mater. Chem. 21 (2011) 5069–5075.
[22] L. Ji, Z. Tan, T.R. Kuykendall, S. Aloni, S. Xun, E. Lin, V. Battaglia, Y. Zhang, Phys. Chem. Chem. Phys. 13 (2011) 7170–7177.
[23] D. Larcher, C. Masquelier, D. Bonnin, Y. Chabre, V. Masson, J.B. Leriche, J.M. Tarascon, J. Electrochem. Soc. 150 (2003) A133–A139.
[24] Y. Nuli, P. Zhang, Z. Guo, H. Liu, J. Electrochem. Soc. 155 (2008) A196–A200.
[25] S. Laurent, D. Forge, M. Port, A. Roch, C. Robic, L.V. Elst, R.N. Muller, Chem. Rev. 108 (2008) 2064–2110.
[26] S.K. Behera, P.K. Sahoo, S.K. Pratihar, S. Bhattacharyya, Mater. Lett. 58 (2004) 3710–3715.
[27] S. Laruelle, S. Grugeon, P. Poizot, M. Dolle, L. Dupont, J.M. Tarascon, J. Electrochem. Soc. 149 (2002) A627.
[28] Y. Yu, C.H. Chen, J.L. Shui, S. Xie, Angew. Chem. Int. Ed. 44 (2005) 7085.
[29] J.S. Chen, Z. Wang, X.C. Dong, P. Chen, X.W.D. Lou, Nanoscale 3 (2011) 2158–2161.
[30] P. Tartaj, M.P. Morales, S. Veintemillas-Verdaguer, T. Gonzalez-Carreno, C.J. Serna, Handbook of Magnetic Materials, Elsevier, Amsterdam, The Netherlands, 2006, p. 403.
[31] K.V.P.M. Shafi, A. Ulman, X. Yan, N.-L. Yang, C. Estournes, H. White, M. Rafailovich, Langmuir 17 (2001) 5093–5097.
[32] J.-P. Jolivet, C. Chaneac, E. Tronc, Chem. Commun. (2004) 481–487.